frontiers | Frontiers in Biomaterials Science

TYPE Original Research
PUBLISHED 17 October 2023
DOI 10.3389/fbiom.2023.1279367

OPEN ACCESS

EDITED BY
Yan Li,
Sun Yat-Sen University, China

REVIEWED BY
Xiao Lin,
Soochow University, China
Raj Kumar,
University of Nebraska Medical Center, United States

*CORRESPONDENCE
Jeffrey R. Capadona,
jrc35@case.edu
Allison Hess-Dunning,
ahess@aptcenter.org

RECEIVED 17 August 2023
ACCEPTED 29 September 2023
PUBLISHED 17 October 2023

CITATION
Kim Y, Druschel LN, Mueller N, Sarno D, Gisser K, Hess-Dunning A and Capadona JR (2023), *In vivo* validation of a mechanically adaptive microfluidic intracortical device as a platform for sustained local drug delivery. *Front. Front. Biomater. Sci.* 2:1279367. doi: 10.3389/fbiom.2023.1279367

In vivo validation of a mechanically adaptive microfluidic intracortical device as a platform for sustained local drug delivery

Youjoung Kim[1,2], Lindsey N. Druschel[1,2], Natalie Mueller[1,2], Danielle Sarno[1,2], Kaela Gisser[1,2], Allison Hess-Dunning[1,2]* and Jeffrey R. Capadona[1,2]*

[1]Department of Biomedical Engineering, Case Western Reserve University, Cleveland, OH, United States, [2]Advanced Platform Technology Center, Louis Stokes Cleveland VA Medical Center, Cleveland, OH, United States

Introduction: Intracortical microelectrodes (IME) are vital to properly functioning brain-computer interfacing (BCI). However, the recording electrodes have shown a steady decline in performance after implantation, mainly due to chronic inflammation. Compliant materials have been explored to decrease differential strain resulting in lower neural inflammation. We have previously developed a fabrication method for creating mechanically adaptive microfluidic probes made of a cellulose nanocrystal (CNC) polymer nanocomposite material that can become compliant after implantation. Here, we hypothesized that our device, would have a similar tissue response to the industry standard, allowing drug delivery therapeutics to improve neural inflammation in the future.

Methods: RNA expression analysis was performed to determine the extent of neural inflammation and oxidative stress in response to the device compared to controls and to naïve shame tissue.

Results: Results presented for both four- and eight-weeks post-implantations suggest that our device offers a promising platform technology that can be used to deliver therapeutic strategies to improve IME performance.

KEYWORDS

intracortical microelectrode, mechanically compliant, microfluidic, *in vivo*, neuroinflammation

1 Introduction

The development of implantable intracortical microelectrodes (IMEs) for brain-computer interfacing (BCI) applications has opened the possibility for patients with spinal cord injury or neural degeneration to regain movement control and improve their quality of life (Schwartz et al., 2006; Shih et al., 2012; Ortiz-Rosario and Adeli, 2013; Thakor, 2013; Jorfi et al., 2015a; Ajiboye et al., 2017). Additionally, IMEs are a valuable tool in science and medicine to explore and map brain regions (Shih et al., 2012; Ortiz-Rosario and Adeli, 2013; Jorfi et al., 2015a). BCIs can encode single neuron activity and translate it to physical movement, increasing patient quality of life (Schwartz et al., 2006; Shih et al., 2012; Ortiz-Rosario and Adeli, 2013; Jorfi et al., 2015a). Unfortunately, studies have shown that most of these implantable devices tend to fail over time, with over half failing within a year of

implantation (Jorfi et al., 2015a; Usoro et al., 2021a; Barrese et al., 2013; Prasad et al., 2012). Explanting or replacing devices is costly and invasive, leading scientists and engineers to explore methods of mitigating failure to improve the quality and longevity of IMEs. Further, being designed for disabled or "locked-in" patients should amplify the need for sustained reliability, as the "cost" of device failure removing restored freedoms is too high of a price for patients to pay.

IME failure has been characterized by the inability to record single neuron activity due to smaller signal amplitude or physical damage to connections (Kipke et al., 2008; Ludwig et al., 2009; Lempka et al., 2011; Jorfi et al., 2015a). Primarily, lower signal quality is driven by biological factors post-implantation, where chronic neuroinflammation leads to neuron death and thick glial scarring (Lempka et al., 2011; Jorfi et al., 2015a; Usoro et al., 2021a). Chronic activation of immune cells such as microglia and macrophages has also been shown to increase resident reactive oxygen species (ROS), resulting in oxidative stress that damages the local cells and corrodes the implanted IME (Potter et al., 2013; Potter et al., 2014; Potter-Baker et al., 2014; Jorfi et al., 2015a; Prasad et al., 2012; Potter-Baker and Capadona, 2015; Potter-Baker et al., 2015; Takmakov et al., 2015; Nguyen et al., 2016; Ereifej et al., 2018; Bennett et al., 2019; Caldwell et al., 2020; Kim et al., 2021a; Ziemba et al., 2022; Chen et al., 2023). To mitigate chronic neuroinflammation, soft substrate materials and drug delivery of anti-inflammatory drugs have been explored (Retterer et al., 2004; Takeuchi et al., 2005; Capadona et al., 2008; Hess et al., 2009; Wester et al., 2009; Hes et al., 2011; Jeon et al., 2014; Nguyen et al., 2014; Apollo et al., 2015; Sridharan et al., 2015; Kim et al., 2017; Scott and Ali, 2021). Nguyen et al. showed that implanting probes made of polymer nanocomposite material compared to stiff silicon probes improved neuronal nuclei density at the probe tissue interface at 4 weeks. By 16 weeks, neuronal density had recovered to background levels (Nguyen et al., 2014). Several subsequent studies have also shown that compliant probes, compared to rigid silicon probes, decrease brain tissue strain and reduce overall inflammation (Harris et al., 2011a; Harris et al., 2011b; Jorfi et al., 2015a; Sridharan et al., 2015). Other materials have also been explored, such as probes made with polydimethylsiloxane (PDMS), parylene-C, or SU-8 (Takeuchi et al., 2004; Takeuchi et al., 2005; Fernández et al., 2009; Altuna et al., 2013; Kim et al., 2017; Luan et al., 2017). Luan et al. were able to create an ultra-flexible probe able to yield single-unit recordings chronically. They showed that the small size and flexibility contributed to glial scar-free neural integration (Luan et al., 2017).

We previously reported on the development of mechanically softening microfluidic neural probes for local drug delivery (Kim et al., 2021b; Kim et al., 2023). This design iteration aimed to at least match the neuroinflammatory response between the platform technology and control (stiff, silicon devices)—to establish a tool for exploring future therapeutics. In that regard, here, we characterized the neuroinflammatory response of our microfluidic dynamically softening neural probe compared to current industry standard silicon probes. Our devices utilize a dynamically softening material, cellulose nanocrystals (CNC) in a polyvinyl acetate (PVAc) matrix that is stiff (5 GPa) to facilitate insertion into brain tissue at room temperature. However, upon insertion and exposure to the aqueous *in vivo* environment, the probe becomes soft (~10 MPa) to decrease the differential strain between the tissue and the device (Capadona et al., 2008; Hess et al., 2009; Hes et al., 2011; Sridharan et al., 2015). Post-mortem analysis was performed on the tissue surrounding the implants to examine differential gene expression for 152 genes involved in oxidative stress and neuroinflammation. Pathway analysis of the significant genes was performed to help elucidate the inflammatory/oxidative stress cascade relationship between experimental and control groups. We hypothesize that when our microfluidic nanocomposite devices deliver local anti-inflammatory therapy, a further decreased expression of inflammatory and oxidative stress genes compared to traditional control probes would be seen. Towards that goal, we first examined the response to the delivery of diluent from the devices to establish that our device would at least have minimal effect on inflammation/oxidative stress compared to traditional probes, establishing its platform capabilities.

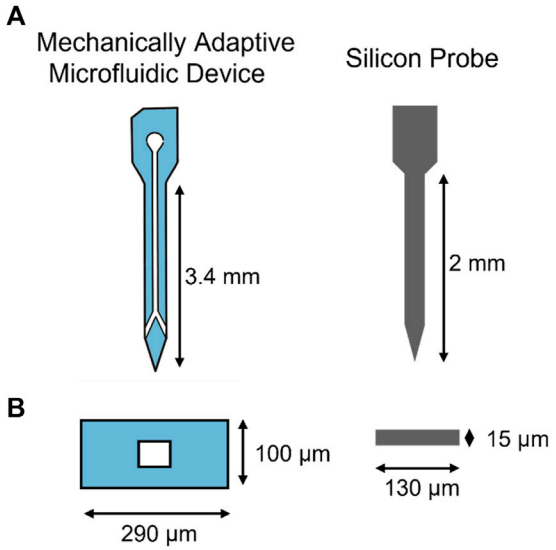

FIGURE 1
Intracortical Microelectrode Probe Designs. Designs for mechanically adaptive microfluidic probes and traditional silicon probes. **(A)** shows the shape of the probes. **(B)** is the cross-sectional view of each probe type.

2 Materials and methods

2.1 Microfluidic probe fabrication methods

Microfluidic dynamically softening probes were fabricated based on previously published works from the lab (Capadona et al., 2008; Hess et al., 2009; Shanmuganathan et al., 2010; Harris et al., 2011a; Harris et al., 2011b; Hes et al., 2011; Sridharan et al., 2015; Kim et al., 2021b; Kim et al., 2023). A photolithographically-defined SU-8 mold of the channel layer film was used to create a negative PDMS mold, which was then placed in a Teflon dish. The cellulose nanocrystals and polyvinyl acetate (PVAc) were dispersed separately in DMF for 6 h and then mixed. The resulting nanocomposite (NC) solution was poured over the PDMS mold, and the solvent was allowed to evaporate in a vacuum oven at 60°C for 1 week. Planar cover layers were made by pouring the NC solution over a flat PDMS slab. After all solvent was evaporated, the films were hot embossed at

90°C for 1 hour while still adhered to the PDMS molds. Deionized water was used to aid in the gentle release of the films from the molds, and the films were then placed in the oven once again for complete drying.

The channel and cover layers were cut into chips consisting of 16 microfluidic channels and 16 outlet holes, respectively, and soaked overnight in DI water to plasticize. The two layers were then aligned and thermally bonded on a hotplate at50°C for 15 min, and then the outer shape of each probe was laser micromachined. The resulting individual probes were connected to custom 3D-printed connectors and PE-50 tubing before sterilizing in cold ethylene oxide gas (Szabo and Hess-Dunning, 2021). Figure 1 shows the dimensions of the mechanically adaptive microfluidic probe compared to the traditional silicon probes.

Study groups requiring fluidic flow used osmotic pumps from Alzet (Durect, 2006 model), which were filled and fitted to the PE-50 tubing end of the completed microfluidic devices in a sterile environment. Resveratrol groups were filled with 30 μM resveratrol in saline, and diluent groups were filled with saline. Each pump was weighed before and after filling to calculate the initial fluid volume. After connection, the microfluidic probe and pump complex was placed in a sterile tube filled with saline to prime the tubing for 60 h pre-implantation.

2.2 Animal surgical methods

All procedures and animal care practices were performed in accordance with the Louis Stokes Department of Veterans Affairs Institutional Animal Care and Use Committees. Male Sprague Dawley rats (225–300 g, Charles River) were used in this study and were allowed to survive for four or 8 weeks after surgery, following previously published studies from our lab (Kim et al., 2021a; Kim et al., 2023). There were three groups [Silicon Control (SC), Nanocomposite Control (NC), and Nanocomposite Diluent (ND)], with five animals per group per time point. No animals were removed, but the eight-week NC group had six animals instead of 5. Silicon control devices are a standard control for rodent studies in this field (Tresco and Winslow, 2011; Karumbaiah et al., 2013; Jorfi et al., 2015b; Usoro et al., 2021b; Thompson et al., 2021).

Briefly, rats were anesthetized with 2.5% isoflurane, and an anesthetic plane was confirmed with a toe pinch. Once anesthetized, the skull area and the mid-scapular regions were shaved and sterilized with alternating betadine and isopropyl alcohol swabs. Pre-operative injections of meloxicam analgesia (1 mg/kg), cefazolin antibiotic (16 mg/kg), and bupivacaine local anesthetic were injected subcutaneously. The rat was then placed on a stereotaxic frame fitted with a nose cone flowing 2.5% isoflurane and 300 mL/h oxygen. The anesthetic plane was rechecked before the initial incision, and vitals were monitored using the Mouse-Stat monitor (Kent Scientific, Torrington, CT, United States).

An incision was made on the scalp, and a cotton-tipped applicator was used to clean the periosteum to expose the skull. Hydrogen peroxide was first applied to dehydrate the skull, and Vetbond (3M, St. Paul, MN, United States) was applied to prime the skull surface for drilling. Craniotomies were made at 3 mm anterior and 3 mm lateral to bregma, using a 1.45 mm drill bit fitted to a Kopf dental drill (David Kopf Instruments, Tujunga, CA, United States). Drilling was done intermittently with saline washes to prevent thermal damage. A subcutaneous pocket was made in the mid-scapular region about 7 cm posterior to place the osmotic pump and the tubing.

Primed microfluidic probes were secured to a stereotaxic frame using a custom holder and lowered 3 mm into the animal's motor cortex. The craniotomy was then sealed with Kwik-Cast (World Precision Instruments, Sarasota, FL, United States) and held in place with a small amount of Teets Cold Cure Dental Cement (A-M Systems, Sequim, WA, United States). The tubing connected to the osmotic pump was also secured using a small amount of dental cement to prevent disconnection of the tube from the pump. Once fully cured, the osmotic pump was implanted into the subcutaneous pocket, and the tubing was cemented into place over the skull as well. Afterward, the probes were disconnected from the custom holder, and a head cap was made of dental cement to secure the whole system into place. The incision was sutured closed, and the animal was monitored for 5 days post-operation. Post-operative injections of meloxicam (1 mg/kg) for pain once a day for 2 days and cefazolin (16 mg/kg) for prophylactic antibiotics twice a day after the surgery.

Chronic time point animals underwent a four-week revision surgery to replace the spent osmotic pumps with newly filled and primed pumps. Animals were anesthetized with 2.5% isoflurane, and the anesthetic plane was confirmed with a toe pinch before the mid-scapular region was shaved and sterilized with alternating betadine and isopropyl alcohol swabs. Preoperative injections of meloxicam for pain and cefazolin for prophylactic antibiotics were injected subcutaneously. Bupivacaine was injected subcutaneously at the incision site for local anesthetic. The animals were placed in the nose cone of the surgical table, flowing 2.5% isoflurane, and another toe pinch was done before the initial incision to ensure an appropriate anesthetic plane. A 1 cm incision was made over the area where the previous osmotic pump was implanted, and the osmotic pump was extracted. The tubing was cut close to the osmotic pump interface to preserve the length of the tubing. The newly filled and primed osmotic pump was fitted to the tubing, and a small amount of dental cement was placed at the tubing/pump interface to ensure the tubing did not disconnect. Once the dental cement was fully cured, the scar capsule was flushed with warm saline, and a new osmotic pump was placed back inside the capsule. The incision was sutured closed, and the animal was observed 5 days postoperatively for signs of complications. Again, the animals were given meloxicam (1 mg/kg) for 2 days, once a day for pain, and cefazolin (16 mg/kg) twice a day for 1 day for a prophylactic antibiotic.

2.3 Explanted osmotic pump eluted volume analysis

Explanted osmotic pumps were placed into a 6-well dish, and the remaining fluid was extracted using a 27 G needle immediately after extraction to limit fluid evaporation. The extracted fluid was quantified using a micropipette and analyzed to determine the average fluid delivery rate and if any animals should be excluded from the study depending on the delivery volume.

TABLE 1 Complete list of neuroinflammatory genes of interest utilized in this study.

Abl1	*C4A*	*Cycs*	*GSTA1*	*Ins2*	*Ngfg*	*Prnp*	*SPP1*
Ager	*C5AR1*	*Ddit3*	*Gsta2*	*Ipcef1*	*Ngfr*	*Psen1*	*Src*
Aif1	*Casp3*	*Dnm2*	*GSTM2*	*IRAK4*	*Nme5*	*PSMB8*	*Srxn1*
AIM2	*CASP8*	*DOCK2*	*Gstp1*	*IRF7*	*Nol3*	*Ptgs2*	*Stx2*
Akt1	*CCL1*	*Ehd2*	*Gucy1b3*	*ITGAM*	*Nos1*	*PTPN6*	*Tbp*
Apoe	*Ccl5*	*Ep300*	*H2-T23*	*Jun*	*Nos3*	*PTX3*	*Tnf*
App	*Ccs*	*Ercc6*	*Hdac2*	*KEAP1*	*Noxa1*	*Rela*	*TNFRSF1A*
ARC	*CD14*	*Fas*	*Hdac6*	*LILRB4A*	*Nqo1*	*Rpl13a*	*TNFRSF25*
Atf4	*CD36*	*FCER1G*	*Hgf*	*Lpo*	*Nr2f6*	*Rps18*	*Tor1a*
Atp13a2	*CD45*	*FCGR2B*	*Hif1a*	*Lrrk2*	*Nr4a2*	*SCD1*	*Tpm1*
Atp7a	*CD68*	*Fn1*	*Hmox1*	*Mapt*	*Osgin1*	*Sdha*	*Trp53*
Atrn	*CD74*	*Fos*	*Hprt*	*Mgmt*	*OSMR*	*SERPINA3N*	*Trpm2*
Bad	*CD84*	*Fxn*	*Hspb1*	*MMP12*	*Oxr1*	*Sirt1*	*Txnl1*
Bcl2	*Cdk2*	*GFAP*	*Htra2*	*Mmp14*	*Park7*	*Sirt2*	*Txnrd1*
Bdnf	*CIM*	*Gnao1*	*Idh1*	*MPEG1*	*Parp1*	*Slc8a1*	*TYROBP*
BLNK	*CLEC7A*	*Gpr37*	*Il1b*	*Mutyh*	*Pdgfrb*	*Snca*	*Ubc*
Bnip3	*Cln8*	*Gsk3b*	*Il1r1*	*Ncf1*	*Pink1*	*Sod1*	*Ubqln1*
C3	*CTSS*	*Gsr*	*IL2RG*	*Nefh*	*Pla2g4a*	*Sod2*	*Vegfa*
C3AR1	*Cybb*	*Gss*	*Il6*	*Nfe2l2*	*Ppargc1a*	*Sod3*	*Xbp1*

Here we list the 152 genes examined in the current study. The custom genes are shown in red, and the preset genes from NanoString are in black. Housekeeping genes are shown in blue and highlighted in gray.

2.4 Perfusion methods

Intraperitoneal (IP) injections of ketamine (80 mg/kg) and xylazine (10 mg/kg) were administered to animals at their respective end time points for transcardial perfusion. The anesthetic plane was confirmed with a toe pinch, and the animals were mounted onto the perfusion tray. A peristaltic pump (VWR International, Radnor, PA, United States) was used to perfuse 500–600 mL 1X PBS and then 400–500 mL 30% sucrose solution at an 8.3 mL/min rate. The brain, head cap, and osmotic pump were collected. The remaining solution in the osmotic pumps was extracted for analysis. The brain was placed in OCT (Optimal Cutting Temperature) Compound Medium (Fisher Scientific, Hampton, NH United States) and flash frozen in dry ice immediately after extraction to protect from RNA degradation.

2.5 RNA isolation and bulk gene analysis

Flash-frozen brains were kept in a −80°C freezer until cryo-slicing. Eight slices of 150 µm thick slices were taken from each brain interspersed with 20 µm and 5 µm thick slices. A 1 mm diameter biopsy punch centered over the implant site on each of the 150 um thick slices were taken and placed into a homogenizing tube (19–627, Soft Tissue Homogenizing Mix 1.4 mm Ceramic 2 mL Tubes, Omni International, Kennesaw GA, United States). All samples were frozen at −80°C until RNA isolation within 24 h.

RNA was extracted and purified from the tissue with the RNeasy Plus Universal Mini Kit (73404, Qiagen, Hilden, Germany) at the Translational Research Shared Resource (TRSR) at the Case Comprehensive Cancer Center. RNA quantity and quality were determined using a Tapestation (Agilent, Santa Clara, CA, United States) and Nanodrop to confirm RNA concentration higher than 20 ng/µL, as required by the nCounter for bulk gene analysis.

Bulk gene expression was done using the nCounter system by NanoString Technologies (Seattle, WA, United States). A 5 µL aliquot of isolated RNA from each sample was hybridized with a CodeSet of capture and reporter probes for a custom panel of inflammation and oxidative stress genes (55 neuroinflammation genes and 97 oxidative stress genes, Table 1). Each sample was incubated for 16 h at 65°C in the thermal cycler and then analyzed using the nCounter MAX Analyzer (NanoString Technologies, Seattle, WA, United States). Gene expression was determined by scanning and counting the fluorescent reporter probes.

2.6 Statistical methods

All sample expression was normalized to 6 housekeeping genes using nSolver software (NanoString Technologies, Seattle, WA, United States). Any gene with less than 20 counts in 85% of samples was removed. Samples were normalized by the geometric mean of spiked in positive control probes. The expression ratio

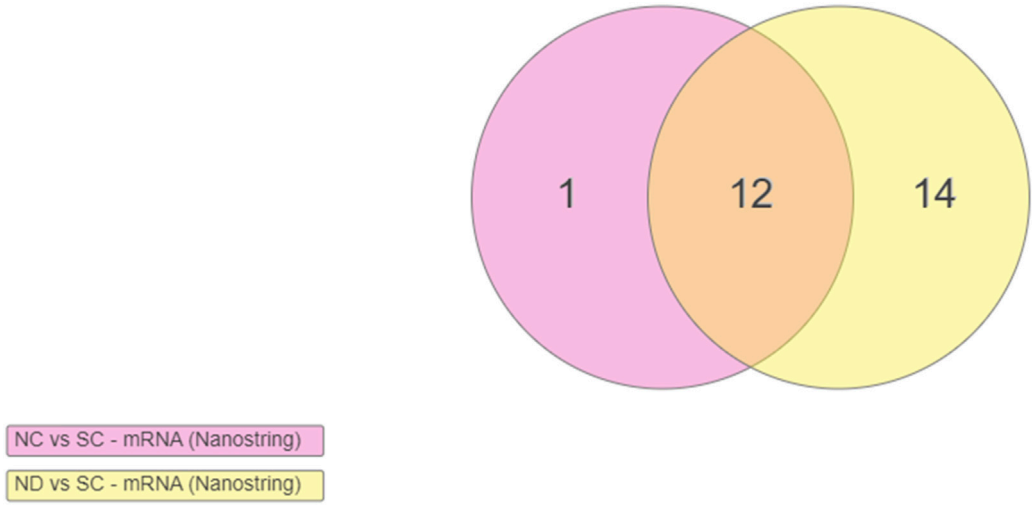

FIGURE 2
Venn diagram indicating the number of differentially expressed genes at 4 weeks post-implantation. Differentially expressed genes in the Nanocomposite (NC) group and the Nanocomposite Diluent (ND) group, compared to Silicon Controls (SC). Comparison of the NC to ND groups provided no significantly differentially expressed genes. Genes are included in the Venn diagram if Log2FoldChange >1 or < −1, $P_{adj} < 0.1$. Overlapping points on the diagram indicate the same genes demonstrating upregulation across both comparisons.

was plotted on a log2 scale and called the Log2FoldChange (Log2FC). Expression of Log2FC = 1 indicates a two-fold increase, whereas Log2FC = −1 indicates a two-fold decrease. Significance was determined using an unpaired *t*-test with Benjamini–Hochberg false discovery rate correction of 10% individually for each group in order to remove genes that might exhibit random significance (Benjamini and Hochberg, 1995).

Volcano plots of expression comparing the silicon control group to experimental groups were created using GraphPad Prism 9 (GraphPad Software, Boston, MA, United States). Venn Diagrams and bar plots were created as a part of iPathwayGuide software for gene pathway analysis. The pathway analysis software iPathwayGuide utilizes impact analysis consisting of the over-representation of differentially expressed genes in a pathway and the perturbation of that pathway.

Groups were compared by first using Silicon Control (SC) as the baseline, thereby creating two comparisons of Nanocomposite Group (NC) vs. SC and Nanocomposite Diluent Group (ND) vs. SC. The two experimental groups were subsequently compared, using NC as a baseline to create the following comparison: ND vs. NC. Therefore, there were a total of three comparisons made per time point. A third experimental group called Nanocomposite Resveratrol (NR) is compared in Supplementary Data Section for 4-week and 8-week comparisons, respectively.

3 Results

3.1 Analysis of explanted osmotic pump eluted volume

Explanted osmotic pumps were evaluated for the amount of total eluted fluids over their given time points, and the fluid flow rate. Pumps explanted from 4 Week ND animals had an average total elution volume of 175 ± 14 μL over the course of 4 weeks. The average flow rate was 0.26 ± 0.02 (μL/hr). The 8 Week animals had two osmotic pumps where the first was explanted at 4 weeks, and replaced with a new filled pump that was explanted at the 8 week time point. The total average fluid volume eluted in the 8 Week ND group was 244 ± 57 μL over the course of 8 weeks. The average flow rate for this group was 0.18 ± 0.04 μL/h. The standard deviation of total elution volume and flow rates were calculated for each animal to determine if any values were above two standard deviations of the mean and should be excluded from the study. No animals exhibited standard deviations above this threshold and were therefore kept in the study for further analysis. All elution volumes and rates were within expected values, verifying fluid delivery.

3.2 Differential gene expression analysis for neuroinflammation

3.2.1 Analysis of 4 Weeks post-implantation

Statistical analysis of the raw gene count values was analyzed to find the Log2FoldChange and *p*-values. The cut-off values were calculated to determine the significantly differentially expressed (upregulated and downregulated) genes compared to the control group. Four weeks post-implantation, a meta-analysis of the experimental groups (Nanocomposite, NC and Nanocomposite Diluent, ND) compared to Silicon Control (SC) groups shows distinct results. First, 13 differentially expressed genes were in the NC group compared to the SC (Figure 2). Eleven of those 13 differentially expressed genes were significantly upregulated, and two were significantly downregulated (Figure 3A). Twelve of the thirteen differentially expressed genes in the NC vs. SC comparison were also differentially expressed in the ND vs. SC comparison (Figure 2). Further, fourteen genes were differentially expressed in the ND vs. SC

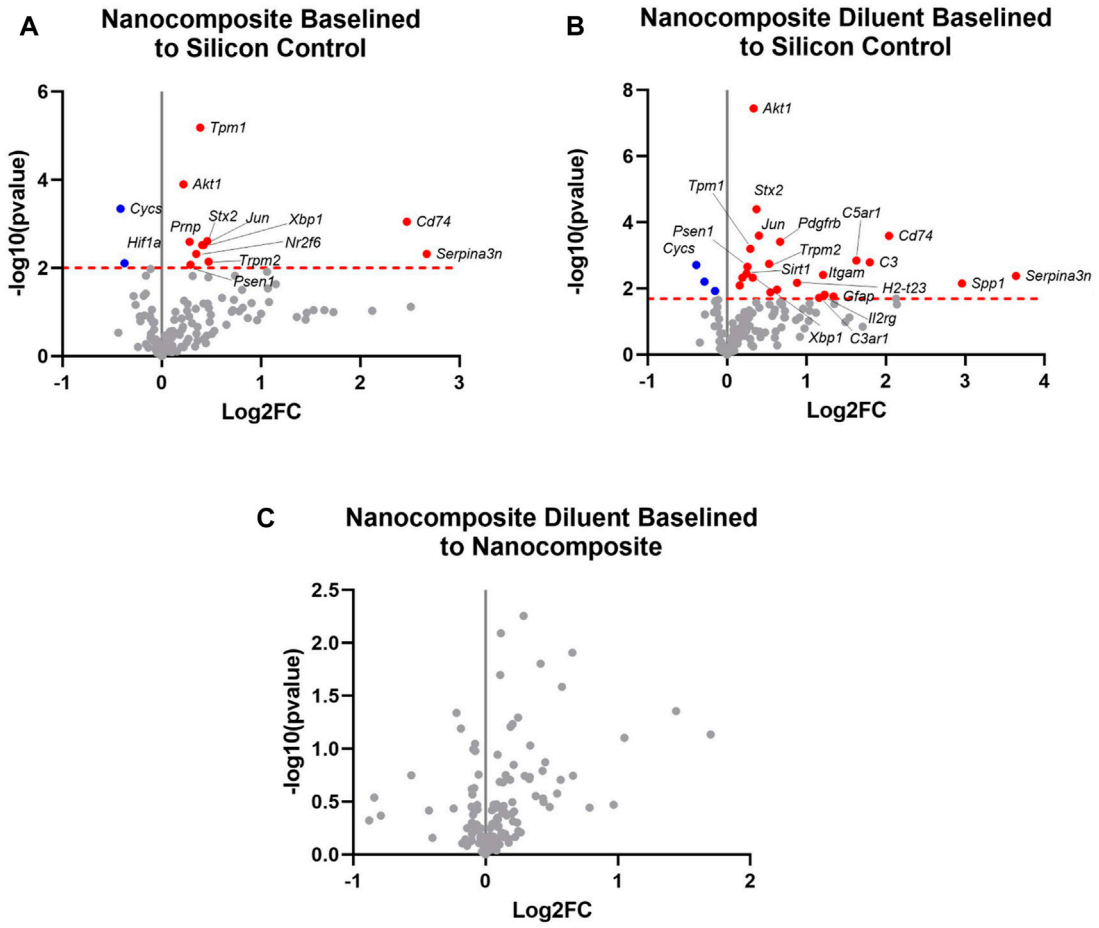

FIGURE 3
Differential expression of neuroinflammatory genes at 4 weeks post-implantation. Volcano plot of the gene expression profiles comparing four-week post-implantation results for **(A)** the Nanocomposite group to the Silicon Control group. Cut-off critical $P_{adj} < 0.1$; **(B)** the Nanocomposite diluent group compared to the Silicon Control group and **(C)** the Nanocomposite Diluent compared to the Nanocomposite group. In all three panels, only the top 20 Log2FC genes in the plots are labeled for simplicity of viewing. Varying groups are plotted against the baseline group in each plot: red is for upregulated genes, and blue is for downregulated genes, all with respect to the "baseline" group. Gray points indicate genes not significantly differentially expressed. Log2FC indicate the fold change of gene expression in the log2 scale. Log2FC = 1 indicates a 2 fold increase in gene expression, whereas Log2FC = −1 indicates 2 fold decrease in gene expression.

comparison (Figure 2). Of the twenty-six genes differentially expressed in the ND vs. SC comparison, twenty-three were upregulated, and three were downregulated (Figure 3B). These results indicate that the NC group only has one uniquely differentially expressed gene compared to ND. However, when we directly compared the NC to the ND group, there were no differentially expressed genes 4 weeks post-implantation (Figure 3C). Comparison of the NC to ND group indicated that the diluent flow through the device into the brain tissue had no appreciable effect on the neuroinflammatory markers examined with our 152 gene panel beyond what was generated from the NC implant alone.

3.2.2 Analysis of 8 Weeks post-implantation

We again performed statistical analysis of the raw gene count values for animals that survived 8 weeks post-implantations to find the Log2FoldChange and *p*-values. The cut-off values were also calculated to determine the significantly differentially expressed (upregulated and downregulated) genes compared to the control group. At 8 weeks post-implantation, a meta-analysis of each of the experimental groups (Nanocomposite, NC and Nanocomposite Diluent, ND) compared to Silicon Control (SC) groups shows no distinct results (Figures 4A, B). Further, a direct comparison of the NC to the ND groups at 8 weeks post-implantation showed none of the examined genes to be differentially expressed (Figure 4C). Our results suggest that the NC and ND probes exhibited an indistinguishable neuroinflammatory gene expression profile from the industry standard SC probes by 8 weeks post-implantation.

As a proof-of-concept experiment, an additional group of animals was treated with Resveratrol, a natural antioxidant that we have used before to minimize oxidative damage and neuroinflammation following microelectrode implantation (Potter et al., 2013; Potter-Baker and Capadona, 2015; Potter-

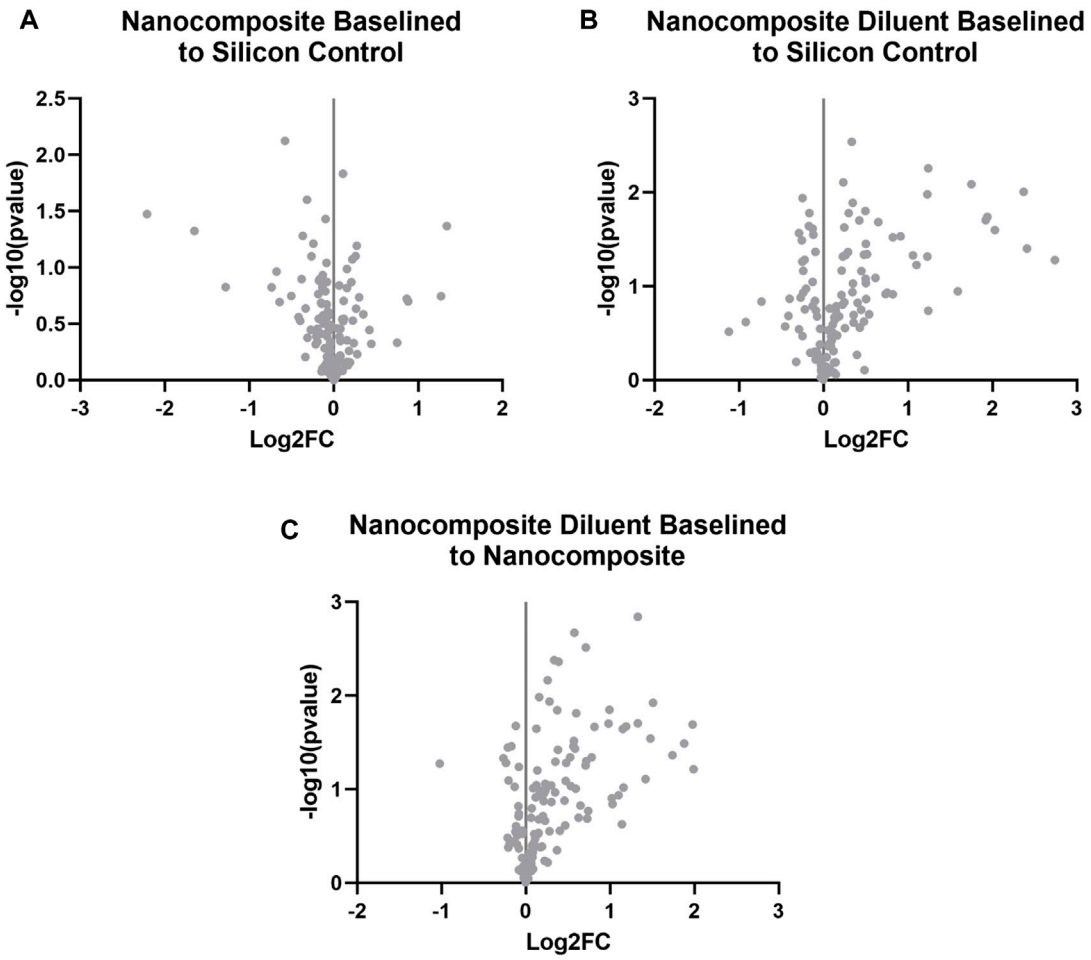

FIGURE 4
Differential expression of neuroinflammatory genes at 8 weeks post-implantation. Volcano plot of the gene expression profiles comparing for 8 weeks post-implantation for **(A)** the Nanocomposite group to the Silicon Control group, **(B)** the Nanocomposite diluent group compared to the Silicon Control group; and **(C)** the Nanocomposite Diluent compared to Nanocomposite group. Varying groups are plotted against the baseline group in each plot: red is for upregulated genes, and blue is for downregulated genes. Up and downregulation is in reference to the baseline group indicated in each title. Gray points are genes that are not significantly up or downregulated. Log2FC indicate the fold change of gene expression in the log2 scale. Log2FC = 1 indicates a 2 fold increase in gene expression, whereas Log2FC = −1 indicates 2 fold decrease in gene expression.

Baker et al., 2015; Nguyen et al., 2016; Haley et al., 2020; Kim et al., 2021b). Resveratrol was loaded into the osmotic pump and delivered through the NC probes throughout the study. Supplementary Figures S1, S2 present the differential gene expression for resveratrol-treated animals at four- and 8 weeks post-implantation. Resveratrol administration resulted in just one differentially upregulated gene, hypoxia-inducible factor-1 (*Hif1a*), 8 weeks post-implantation. *Hif1a* is part of the hypoxia-inducible factor-1 heterodimer that has been shown to regulate cellular and systemic homeostatic response to hypoxia by activating the transcription of many genes. Genes shown to be impacted by *Hif1* expression levels include those involved in energy metabolism, angiogenesis, apoptosis, and other genes whose protein products increase oxygen delivery or facilitate metabolic adaptation to hypoxia–all of which would be expected to be differentially regulated following a hypoxic injury treated with an antioxidant.

3.3 Pathway analysis

To better understand the implications and connections between the differential gene expression in this study, and the known roles of the genes investigated here, we utilized a bioinformatics software package called iPathwayGuide, by Advaita. iPathwayGuide provides a user-friendly interface to investigate the genes of interest. Since the eight-week differential gene expression showed no significant differences (Figure 4), we only completed the iPathwayGuide analysis for the 4 week time point.

3.3.1 Analysis of nanocomposite group vs. silicon controls at 4 weeks

Here, we started by first investigating the significance of differentially expressed genes in comparing the NC group to the SC group at 4 weeks. The iPathwayGuide analysis indicated three significantly impacted pathways: spinocerebellar ataxia,

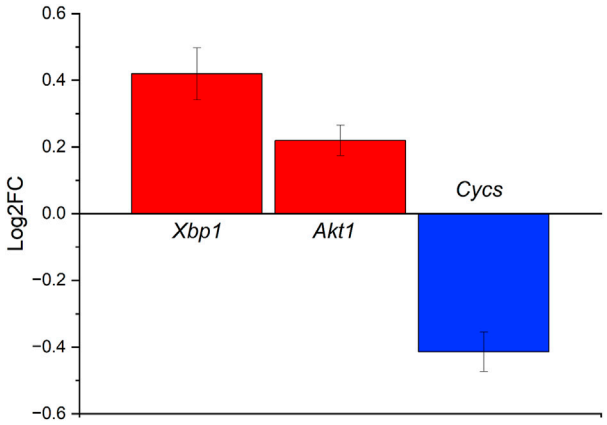

FIGURE 5
Differentially expressed genes in the spinocerebellar ataxia pathway ranked based on Log2FC change for the NC vs. SC groups at 4 weeks post-implantation. *Cycs* is shown to be downregulated, while *Xbp1* and *Akt1* are upregulated slightly.

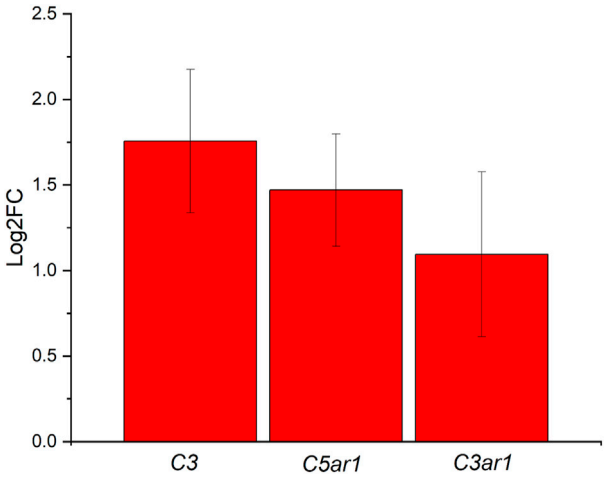

FIGURE 6
Differentially expressed genes in the Neuroactive ligand-receptor pathway for ND vs. SC at 4 weeks post-implantations were ranked based on Log2FC. All three genes are shown to be upregulated.

choline metabolism in cancer, and PD-L1 expression and PD-1 checkpoint. Due to the relevance to neuroinflammation and oxidative stress in the central nervous system, only the spinocerebellar ataxia pathway will be discussed here.

Spinocerebellar ataxias are a group of neurodegenerative diseases characterized by loss of motor coordination. The causes include transcriptional dysregulation, protein aggregation, and mitochondria defects, leading to apoptosis (Lastres-Becker et al., 2008). Of the 13 genes that were differentially expressed between the NC and SC groups at 4 weeks post-implantation, three can be found in the spinocerebellar ataxias pathway Cytochrome C, Somatic (*Cycs*), X-Box Binding Protein 1 (*Xbp1*), and AKT Serine/Threonine Kinase 1 (*Akt1*) (Figure 5). *Cycs*, *Xbp1*, and *Akt1* are all implicated in protein modulation and coding, and perturbations may lead to apoptosis (Chen et al., 2001; Chen and Goeddel, 2002; Urwin et al., 2002; Xiromerisiou et al., 2008; Uchiyama et al., 2018; Park et al., 2021). *Cycs* was downregulated while *Xbp1*, and *Akt1* were upregulated (Figure 5). The *Cycs* and *Akt1* genes are also involved in the Tumor Necrosis Factor (TNF) pathways which are heavily implicated in inflammation and immunity (Chen and Goeddel, 2002; Urwin et al., 2002; Xiromerisiou et al., 2008; Uchiyama et al., 2018). When *Cycs*, *Xbp1*, and *Akt1* are put into context, they show that: 1) *Xbp1* increases the Endoplasmic Reticulum (ER) Stress response, which occurs when the ability of the endoplasmic reticulum to fold proteins becomes saturated and signals cell death, leading to impaired cellular processes; 2) *Akt1* upregulation inhibits Purkinje cell migration abilities; and 3) *Cycs* downregulation contributes to the progression of spinocerebellar ataxia type 2 (SCA2), which has been shown to manifest as the neurodegenerative diseases–cerebellar syndrome and Parkinson's syndrome (Lastres-Becker et al., 2008; Lin et al., 2008).

3.3.2 Analysis of nanocomposite diluent group vs. silicon controls at 4 weeks

The iPathwayGuide analysis of the comparison in gene expression for the Nanocomposite Diluent (ND) group compared to Silicon control (SC) showed five significantly impacted pathways. However, due to the relevance of pathways associated with inflammation in the brain, only the neuroactive ligand-receptor interaction pathway, JAK-STAT signaling, complement and coagulation cascade, and spinocerebellar ataxia pathways will be discussed.

The Neuroactive ligand-receptor interaction pathway consists of receptors and ligands on cellular membranes involved with intra and extracellular signaling pathways (Wei et al., 2020). Genes that were differentially expressed in our study and are also a part of the neuroactive ligand-receptor interaction pathway include Complement C3a (*C3a*), which interacts with the Complement C3a-Receptor (*C3ar*) and Complement C5 receptor (*C5r*) (Boackle, 2019). These three genes were upregulated for ND probes compared to SC (Figure 6). These three genes are part of the complement system and can trigger degranulation of endothelial cells, mast cells, or phagocytes (Bokisch et al., 1969; Takabayashi et al., 1996; Coulthard and Woodruff, 2015). The upregulation of *C3a*, *C3ar*, *and C5r* is understandable since the size difference between the NC and ND probes was much larger than the silicon probes. The plot shows the fold change of those three genes discussed using SC as baseline.

The second pathway that was indicated in our iPathwayGuide analysis for the ND vs. SC comparison was the JAK-STAT signaling pathway. The JAK-STAT signaling pathway is one of the primary mechanisms for cytokine and growth factor regulation (Nicolas et al., 2013; Rusek et al., 2023). Upregulated genes include Glial Fibrillary Acidic Protein (*Gfap*), Interleukin 2 Receptor Subunit Gamma (*Il2rg*), Platelet Derived Growth Factor Receptor Beta (*Pdgfrb*), Protein Tyrosine Phosphatase Non-Receptor Type 6 (*Ptpn6*), and AKT Serine/Threonine Kinase 1 (*Akt1*) (Figure 7). These genes have been implicated in the upregulation of the receptors responsible for the cytokine interaction, which ultimately causes downstream effects in cell cycle behavior (Nicolas et al., 2013; Rusek et al., 2023). Cell cycle behavior changes may affect cell survival, inducing apoptosis if disturbed.

The third pathway indicated in our iPathwayGuide analysis for the ND vs. SC comparison was the spinocerebellar ataxia pathway.

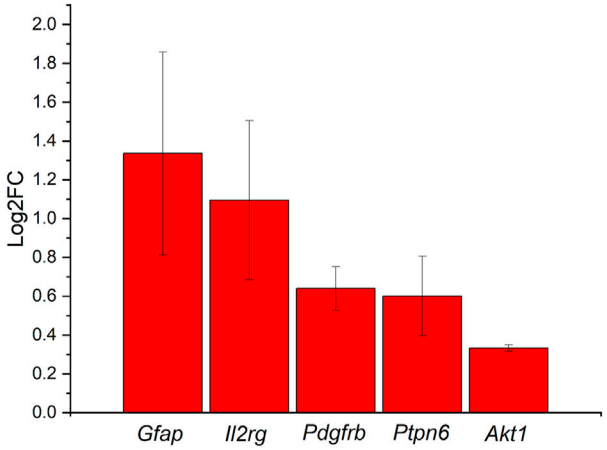

FIGURE 7
Differentially expressed genes in the JAK-STAT signaling pathway in comparison between ND group vs. SC groups at 4 weeks ranked on the Log2FC. All genes are shown to be upregulated, with *Gfap* and *Il2rg* having at least a 2-fold increase, *Pdgfrb* and *Ptpn6* with at least 1-fold increase, and *Akt1* with at less than 1-fold increase.

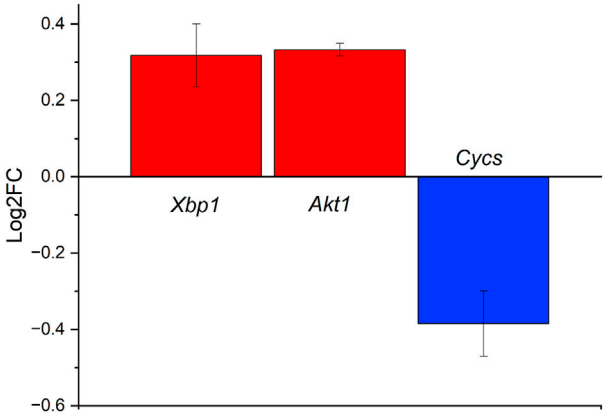

FIGURE 8
Differentially expressed genes in the spinocerebellar pathway ranked based on Log2FC for the ND vs. SC groups at 4 weeks post-implantation. *Cycs* is observed to be downregulated slightly, while *Akt1* and *Xbp1* are upregulated slightly.

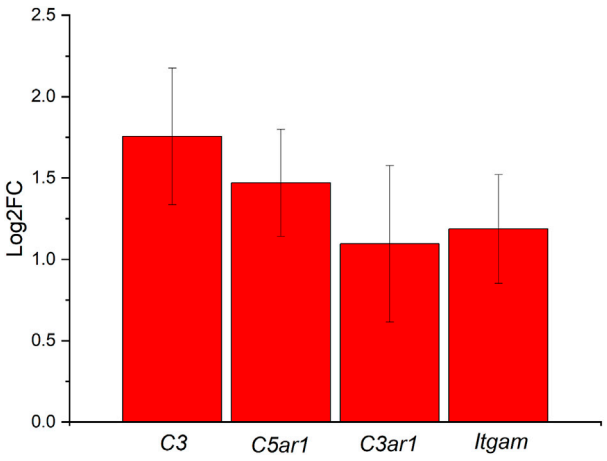

FIGURE 9
Differentially expressed genes in the Complement and Coagulation Cascade ranked based on Log2FC for the ND vs. SC groups at 4 weeks post-implantation. Differentially expressed genes include *C3*, *C5ar1*, *Itgam*, and *C3ar1*, *all* upregulated at least 2-fold.

We have already discussed this pathway in the context of the NC vs. the SC. As described previously, the spinocerebellar ataxia pathway is involved with progressive neurodegenerative diseases (Tresco and Winslow, 2011). Here, we are comparing the ND to the SC control. The difference between this comparison to the earlier comparison is the addition of the diluent being released from the probe. As indicated in the comparison between the ND and NC conditions (Figure 2), the release of diluent fluid does not result in significant differences in differential gene expression. Therefore, the iPathwayGuide analysis for the spinocerebellar ataxia pathway highlighted the same three genes for ND vs. SC as did the NC vs. SC analysis (Figure 8); *Cycs*, *Akt1*, and *Xbp1*.

The last significant pathway identified during the iPathwayGuide analysis was the complement and coagulation cascades. Our lab is currently exploring the complement pathway, as it is the primary regulator of innate immunity. Coagulation is also implicated in the inflammatory processes and is relevant to the implantation of intracortical probes due to the vascular trauma that occurs during the implantation process (Ravikumar et al., 2014; Goss-Varley et al., 2017; Bedell et al., 2018a; Shoffstall et al., 2018a; Bedell et al., 2018b; Shoffstall et al., 2018b; Didar et al., 2022; Hoeferlin et al., 2022; Lam et al., 2023). Here, differentially expressed genes from our analysis of the ND vs. SC groups at 4 weeks post-implantation included Complement C3 (*C3*), Complement C5a Receptor 1 (*C5ar1*), Integrin Subunit Alpha M (*Itgam*), and Complement C3a Receptor 1 (*C3ar1*). All these genes demonstrated increased expression in the ND group compared to the SC group (Figure 9). The downstream effects of *C3*, *C5ar1*, *Itgam*, and *C3ar1* upregulation include increased degranulation, chemotaxis, and phagocytosis (Bokisch et al., 1969; Coulthard and Woodruff, 2015).

4 Discussion

Chronically, at 8 weeks post-implantation, there were no significantly differentially expressed genes when comparing the NC to SC or ND to SC (Figure 4). The lack of significantly differentially expressed genes at 8 weeks demonstrates that our designs are at least as compatible as the static, industry-standard laminar silicon probe before employing the added capability of local therapeutic delivery.

When comparing the ND group to the NC group, there were also no significantly differentially expressed genes at four or 8 weeks post-implantations (Figures 3C, 4C), indicating that including fluid flow to the device does not change the neuroinflammatory response. Demonstration that the influx of flow from the osmotic pump through the microfluidic channels is significant. Several studies have suggested that the blood-brain barrier breakdown and the resulting edema local to the implant site can contribute to sustained, self-perpetuating neuroinflammatory

responses to implanted microelectrode arrays (Scherrmann, 2002; Hammarlund-Udenaes et al., 2008; Foley et al., 2009; Dong, 2018; Kim et al., 2021a). Again, the lack of differential response when directly comparing the ND and NC groups validates the ability of therapeutic delivery without causing further damage due to the fluid mechanics of the solutions or pressure build-up at the device-tissue interface. Notably, the similarity in the response between the ND and NC groups was seen at the more dynamically changing acute phase (4 weeks post-implantation, Figure 3C) and the more stable chronic phase (8 weeks post-implantation, Figure 4C).

5 Conclusion

Here we report on the initial histological evaluation of chronically deployable microfluidic mechanically adaptive polymer IME implants. While some inflammation existed at 4 weeks post-implantation, by 8 weeks post-implantations, there was an almost negligible increase in differentially expressed inflammatory genes in the experimental groups compared to controls. The lack of differentially expressed inflammatory genes at the chronic time indicates that our device is not significantly different from traditional silicon probes–suggesting that with the incorporation of a selected neuroinflammatory agent, our device will become capable of limiting neuroinflammation. Our novel system presents exciting opportunities to be used as a platform technology to implement complex therapeutic delivery strategies in future studies. Anti-inflammatory drugs, antioxidants, or other immune modulatory therapies may be delivered chronically with varying time points due to the replaceable nature of the osmotic pump. The pump may be removed at specific time points and replaced with a new one filled with a different drug or dosage to target various steps along the inflammatory cascade. Such studies offer an exciting opportunity to investigate therapeutics' direct impact correlated with a time scale and dosage.

Data availability statement

The original contributions presented in the study are included in the article/Supplementary Material, further inquiries can be directed to the corresponding authors.

Ethics statement

The animal study was approved by the Louis Stokes Cleveland Department of Veterans Affairs IACUC. The study was conducted in accordance with the local legislation and institutional requirements.

Author contributions

YK: Formal Analysis, Investigation, Methodology, Writing–original draft. LD: Data curation, Formal Analysis, Investigation, Writing–review and editing. NM: Investigation, Methodology, Writing–review and editing. DS: Data curation, Investigation, Writing–review and editing. KG: Data curation, Investigation, Writing–review and editing. AH-D: Conceptualization, Data curation, Funding acquisition, Investigation, Project administration, Resources, Supervision, Validation, Writing–review and editing. JC: Conceptualization, Funding acquisition, Investigation, Project administration, Resources, Supervision, Validation, Writing–review and editing.

Funding

The authors declare financial support was received for the research, authorship, and/or publication of this article. This research was funded by the Merit Review Award I01RX003083 (AH-D) and a Senior Research Career Scientist Award, IK6RX003077 (JC) from the United States Department of Veterans Affairs Rehabilitation Research and Development Service. Additional support was provided in a pre-doctoral fellowship to YK from the National Institute for Biomedical Imaging and Bioengineering, T32EB004314 (JC).

Acknowledgments

We would like to acknowledge Translational Research Shared Resource (TRSR) at the Case Comprehensive Cancer Center for their help in methodology. We would also like to acknowledge Dr. Christian Zorman for use of his laboratory space.

Conflict of interest

The authors declare that the research was conducted in the absence of any commercial or financial relationships that could be construed as a potential conflict of interest.

The authors declared that they were an editorial board member of Frontiers, at the time of submission. This had no impact on the peer review process and the final decision.

Publisher's note

Supplementary material

The Supplementary Material for this article can be found online at: https://www.frontiersin.org/articles/10.3389/fbiom.2023.1279367/full#supplementary-material

References

Ajiboye, A. B., Willett, F. R., Young, D. R., Memberg, W. D., Murphy, B. A., Miller, J. P., et al. (2017). Restoration of reaching and grasping movements through brain-controlled muscle stimulation in a person with tetraplegia: a proof-of-concept demonstration. *Lancet* 389 (10081), 1821–1830. doi:10.1016/s0140-6736(17)30601-3

Altuna, A., Bellistri, E., Cid, E., Aivar, P., Gal, B., Berganzo, J., et al. (2013). SU-8 based microprobes for simultaneous neural depth recording and drug delivery in the brain. *Lab a Chip* 13 (7), 1422–1430. doi:10.1039/c3lc41364k

Apollo, N. V., Maturana, M. I., Tong, W., Nayagam, D. A. X., Shivdasani, M. N., Foroughi, J., et al. (2015). Soft, Flexible Freestanding Neural Stimulation and Recording Electrodes Fabricated from Reduced Graphene Oxide. *Adv. Funct. Mater.* 25 (23), 3551–3559. doi:10.1002/adfm.201500110

Barrese, J. C., Rao, N., Paroo, K., Triebwasser, C., Vargas-Irwin, C., Franquemont, L., et al. (2013). Failure mode analysis of silicon-based intracortical microelectrode arrays in non-human primates. *J. Neural Eng.* 10 (6), 066014. doi:10.1088/1741-2560/10/6/066014

Bedell, H. W., Hermann, J. K., Ravikumar, M., Lin, S., Rein, A., Li, X., et al. (2018a). Targeting CD14 on blood derived cells improves intracortical microelectrode performance. *Biomaterials* 163, 163–173. doi:10.1016/j.biomaterials.2018.02.014

Bedell, H. W., Song, S., Li, X., Molinich, E., Lin, S., Stiller, A., et al. (2018b). Understanding the Effects of Both CD14-Mediated Innate Immunity and Device/Tissue Mechanical Mismatch in the Neuroinflammatory Response to Intracortical Microelectrodes. *Front. Neurosci.* 12, 772. doi:10.3389/fnins.2018.00772

Benjamini, Y., and Hochberg, Y. (1995). Controlling the false discovery rate: a practical and powerful approach to multiple testing. *J. R. Stat. Soc. Ser. B Methodol.* 57 (1), 289–300. doi:10.1111/j.2517-6161.1995.tb02031.x

Bennett, C., Mohammed, F., Álvarez-Ciara, A., Nguyen, M. A., Dietrich, W. D., Rajguru, S. M., et al. (2019). Neuroinflammation, oxidative stress, and blood-brain barrier (BBB) disruption in acute Utah electrode array implants and the effect of deferoxamine as an iron chelator on acute foreign body response. *Biomaterials* 188, 144–159. doi:10.1016/j.biomaterials.2018.09.040

Boackle, S. A. (2019). "The Role of Complement in SLE," in *Dubois' lupus erythematosus and related syndromes* (Amsterdam, Netherlands: Elsevier), 224–236.

Bokisch, V. A., Muller-Eberhard, H. J., and Cochrane, C. G. (1969). Isolation of a fragment (C3a) of the third component of human complement containing anaphylatoxin and chemotactic activity and description of an anaphylatoxin inactivator of human serum. *J. Exp. Med.* 129 (5), 1109–1130. doi:10.1084/jem.129.5.1109

Caldwell, R., Street, M. G., Sharma, R., Takmakov, P., Baker, B., and Rieth, L. (2020). Characterization of Parylene-C degradation mechanisms: *in vitro* reactive accelerated aging model compared to multiyear *in vivo* implantation. *Biomaterials* 232, 119731. doi:10.1016/j.biomaterials.2019.119731

Capadona, J. R., Shanmuganathan, K., Tyler, D. J., Rowan, S. J., and Weder, C. (2008). Stimuli-Responsive Polymer Nanocomposites Inspired by the Sea Cucumber Dermis. *Science* 319 (5868), 1370–1374. doi:10.1126/science.1153307

Chen, G., and Goeddel, D. V. (2002). TNF-R1 Signaling: A Beautiful Pathway. *Science* 296 (5573), 1634–1635. doi:10.1126/science.1071924

Chen, R., Funnell, J. L., Quinones, G. B., Bentley, M., Capadona, J. R., Gilbert, R. J., et al. (2023). Poly(pro-curcumin) Materials Exhibit Dual Release Rates and Prolonged Antioxidant Activity as Thin Films and Self-Assembled Particles. *Biomacromolecules* 24 (1), 294–307. doi:10.1021/acs.biomac.2c01135

Chen, W. S., Xu, P. Z., Gottlob, K., Chen, M. L., Sokol, K., Shiyanova, T., et al. (2001). Growth retardation and increased apoptosis in mice with homozygous disruption of the akt1 gene. *Genes and Dev.* 15 (17), 2203–2208. doi:10.1101/gad.913901

Coulthard, L. G., and Woodruff, T. M. (2015). Is the Complement Activation Product C3a a Proinflammatory Molecule? Re-evaluating the Evidence and the Myth. *J. Immunol.* 194 (8), 3542–3548. doi:10.4049/jimmunol.1403068

Didar, U., Swingle, K., Girish, A., Luc, N., La Fuente, M., Alvikas, J., et al. (2022). Platelet-mimicking procoagulant nanoparticles augment hemostasis in animal models of bleeding. *Sci. Transl. Med.*, 8975. doi:10.1126/scitranslmed.abb8975

Dong, X. (2018). Current Strategies for Brain Drug Delivery. *Theranostics* 8 (6), 1481–1493. doi:10.7150/thno.21254

Ereifej, E. S., Rial, G. M., Hermann, J. K., Smith, C. S., Meade, S. M., Rayyan, J. M., et al. (2018). Implantation of neural probes in the brain elicits oxidative stress. *Front. Bioeng. Biotechnol.* 6, 9. doi:10.3389/fbioe.2018.00009

Fernández, L. J., Altuna, A., Tijero, M., Gabriel, G., Villa, R., Rodríguez, M. J., et al. (2009). Study of functional viability of SU-8-based microneedles for neural applications. *J. Micromechanics Microengineering* 19 (2), 025007–25007. doi:10.1088/0960-1317/19/2/025007

Foley, C. P., Nishimura, N., Neeves, K. B., Schaffer, C. B., and Olbricht, W. L. (2009). Flexible microfluidic devices supported by biodegradable insertion scaffolds for convection-enhanced neural drug delivery. *Biomed. Microdevices* 11 (4), 915–924. doi:10.1007/s10544-009-9308-6

Goss-Varley, M., Dona, K. R., McMahon, J. A., Shoffstall, A. J., Ereifej, E. S., Lindner, S. C., et al. (2017). Microelectrode implantation in motor cortex causes fine motor deficit: implications on potential considerations to Brain Computer Interfacing and Human Augmentation. *Sci. Rep.* 7 (1), 15254–15312. doi:10.1038/s41598-017-15623-y

Haley, R. M., Zuckerman, S. T., Dakhlallah, H., Capadona, J. R., von Recum, H. A., and Ereifej, E. S. (2020). Resveratrol delivery from implanted cyclodextrin polymers provides sustained antioxidant effect on implanted neural probes. *Int. J. Mol. Sci.* 21 (10), 3579. doi:10.3390/ijms21103579

Hammarlund-Udenaes, M., Fridén, M., Syvänen, S., and Gupta, A. (2008). On The Rate and Extent of Drug Delivery to the Brain. *Pharm. Res.* 25 (8), 1737–1750. doi:10.1007/s11095-007-9502-2

Harris, J. P., Capadona, J. R., Miller, R. H., Healy, B. C., Shanmuganathan, K., Rowan, S. J., et al. (2011a). Mechanically adaptive intracortical implants improve the proximity of neuronal cell bodies. *J. Neural Eng.* 8 (6), 066011–66011. doi:10.1088/1741-2560/8/6/066011

Harris, J. P., Hess, A. E., Rowan, S. J., Weder, C., Zorman, C. A., Tyler, D. J., et al. (2011b). *In vivo* deployment of mechanically adaptive nanocomposites for intracortical microelectrodes. *J. Neural Eng.* 8 (4), 046010. doi:10.1088/1741-2560/8/4/046010

Hess, A. E., Capadona, J. R., Shanmuganathan, K., Hsu, L., Rowan, S. J., Weder, C., et al. (2011). Development of a stimuli-responsive polymer nanocomposite toward biologically optimized, MEMS-based neural probes. *J. Micromechanics Microengineering* 21 (5), 054009–54009. doi:10.1088/0960-1317/21/5/054009

Hess, A., Dunning, J., Harris, J., Capadona, J. R., Shanmuganathan, K., Rowan, S. J., et al. (2009). "A bio-inspired, chemo-responsive polymer nanocomposite for mechanically dynamic microsystems," in Proceedings of the TRANSDUCERS 2009 - 2009 International Solid-State Sensors, Actuators and Microsystems Conference, Denver, CO, USA, June 2009 (IEEE).

Hoeferlin, G. F., Menendez, D. M., Krebs, O. K., Capadona, J. R., and Shoffstall, A. J. (2022). Assessment of Thermal Damage from Robot-Drilled Craniotomy for Cranial Window Surgery in Mice. *J. Vis. Exp.* doi:10.3791/64188

Jeon, M., Cho, J., Kim, Y. K., Jung, D., Yoon, E. S., Shin, S., et al. (2014). Partially flexible MEMS neural probe composed of polyimide and sucrose gel for reducing brain damage during and after implantation. *J. Micromechanics Microengineering* 24 (2), 025010. doi:10.1088/0960-1317/24/2/025010

Jorfi, M., Skousen, J. L., Weder, C., and Capadona, J. R. (2015a). "Progress towards biocompatible intracortical microelectrodes for neural interfacing applications," in *Journal of neural engineering* (Bristol, England: Institute of Physics Publishing).

Jorfi, M., Skousen, J. L., Weder, C., and Capadona, J. R. (2015b). Progress towards biocompatible intracortical microelectrodes for neural interfacing applications. *J. Neural Eng.* 12 (1), 011001. doi:10.1088/1741-2560/12/1/011001

Karumbaiah, L., Saxena, T., Carlson, D., Patil, K., Patkar, R., Gaupp, E. A., et al. (2013). Relationship between intracortical electrode design and chronic recording function. *Biomaterials* 34 (33), 8061–8074. doi:10.1016/j.biomaterials.2013.07.016

Kim, A. A., Kustanovich, K., Baratian, D., Ainla, A., Shaali, M., Jeffries, G. D. M., et al. (2017). SU-8 free-standing microfluidic probes. *Biomicrofluidics* 11 (1), 014112. doi:10.1063/1.4975026

Kim, Y., Ereifej, E. S., Schwartzman, W. E., Meade, S. M., Chen, K., Rayyan, J., et al. (2021a). Investigation of the Feasibility of Ventricular Delivery of Resveratrol to the Microelectrode Tissue Interface. *Micromachines* 12 (12), 1446. doi:10.3390/mi12121446

Kim, Y., Mueller, N., Schwartzman, W., Aluri, V., Herried, A., Capadona, J. R., et al. (2021b). "Hybrid Fabrication Method for Microfluidic Channels within a Polymer Nanocomposite for Neural Interfacing Applications," in Proceedings of the 21st International Conference on Solid-State Sensors, Actuators and Microsystems, TRANSDUCERS, Orlando, FL, USA, June 2021 (Institute of Electrical and Electronics Engineers Inc).

Kim, Y., Mueller, N. N., Schwartzman, W. E., Sarno, D., Wynder, R., Hoeferlin, G. F., et al. (2023). Fabrication Methods and Chronic *In Vivo* Validation of Mechanically Adaptive Microfluidic Intracortical Devices. *Micromachines* 14 (5), 1015. doi:10.3390/mi14051015

Kipke, D. R., Shain, W., Buzsáki, G., Fetz, E., Henderson, J. M., Hetke, J. F., et al. (2008). Advanced Neurotechnologies for Chronic Neural Interfaces: new Horizons and Clinical Opportunities. *J. Neurosci.* 28 (46), 11830–11838. doi:10.1523/jneurosci.3879-08.2008

Lam, D. V., Javadekar, A., Patil, N., Yu, M., Li, L., Menendez, D. M., et al. (2023). Platelets and hemostatic proteins are co-localized with chronic neuroinflammation surrounding implanted intracortical microelectrodes. *Acta Biomater.* 166, 278–290. doi:10.1016/j.actbio.2023.05.004

Lastres-Becker, I., Rüb, U., and Auburger, G. (2008). Spinocerebellar ataxia 2 (SCA2). *Cerebellum* 7 (2), 115–124. doi:10.1007/s12311-008-0019-y

Lempka, S. F., Johnson, M. D., Moffitt, M. A., Otto, K. J., Kipke, D. R., and McIntyre, C. C. (2011). Theoretical analysis of intracortical microelectrode recordings. *J. neural Eng.* 8 (4), 045006. doi:10.1088/1741-2560/8/4/045006

Lin, J. H., Walter, P., and Yen, T. S. B. (2008). Endoplasmic Reticulum Stress in Disease Pathogenesis. *Annu. Rev. Pathology Mech. Dis.* 3 (1), 399–425. doi:10.1146/annurev.pathmechdis.3.121806.151434

Luan, L., Wei, X., Zhao, Z., Siegel, J. J., Potnis, O., Tuppen, C. A., et al. (2017). Ultraflexible nanoelectronic probes form reliable, glial scar–free neural integration. *Sci. Adv.* 3 (2), e1601966. doi:10.1126/sciadv.1601966

Ludwig, K. A., Miriani, R. M., Langhals, N. B., Joseph, M. D., Anderson, D. J., and Kipke, D. R. (2009). Using a common average reference to improve cortical neuron recordings from microelectrode arrays. *J. Neurophysiology* 101 (3), 1679–1689. doi:10.1152/jn.90989.2008

Nguyen, J. K., Jorfi, M., Buchanan, K. L., Park, D. J., Foster, E. J., Tyler, D. J., et al. (2016). Influence of resveratrol release on the tissue response to mechanically adaptive cortical implants. *Acta Biomater.* 29, 81–93. doi:10.1016/j.actbio.2015.11.001

Nguyen, J. K., Park, D. J., Skousen, J. L., Hess-Dunning, A. E., Tyler, D. J., Rowan, S. J., et al. (2014). Mechanically-compliant intracortical implants reduce the neuroinflammatory response. *J. Neural Eng.* 11 (5), 056014. doi:10.1088/1741-2560/11/5/056014

Nicolas, C. S., Amici, M., Bortolotto, Z. A., Doherty, A., Csaba, Z., Fafouri, A., et al. (2013). The role of JAK-STAT signaling within the CNS. *JAK-STAT* 2 (1), e22925. doi:10.4161/jkst.22925

Ortiz-Rosario, A., and Adeli, H. (2013). Brain-computer interface technologies: from signal to action. *Rev. Neurosci.* 24 (5), 537–552. doi:10.1515/revneuro-2013-0032

Park, S.-M., Kang, T.-I., and So, J.-S. (2021). Roles of XBP1s in Transcriptional Regulation of Target Genes. *Biomedicines* 9 (7), 791. doi:10.3390/biomedicines9070791

Potter, K. A., Buck, A. C., Self, W. K., Callanan, M. E., Sunil, S., and Capadona, J. R. (2013). The effect of resveratrol on neurodegeneration and blood brain barrier stability surrounding intracortical microelectrodes. *Biomaterials* 34 (29), 7001–7015. doi:10.1016/j.biomaterials.2013.05.035

Potter, K. A., Jorfi, M., Householder, K. T., Foster, E. J., Weder, C., and Capadona, J. R. (2014). Curcumin-releasing mechanically adaptive intracortical implants improve the proximal neuronal density and blood–brain barrier stability. *Acta Biomater.* 10 (5), 2209–2222. doi:10.1016/j.actbio.2014.01.018

Potter-Baker, K. A., and Capadona, J. R. (2015). Reducing the "Stress": antioxidative Therapeutic and Material Approaches May Prevent Intracortical Microelectrode Failure. *ACS Macro Lett.* 4 (3), 275–279. doi:10.1021/mz500743a

Potter-Baker, K. A., Nguyen, J. K., Kovach, K. M., Gitomer, M. M., Srail, T. W., Stewart, W. G., et al. (2014). Development of superoxide dismutase mimetic surfaces to reduce accumulation of reactive oxygen species for neural interfacing applications. *J. Mater. Chem. B* 2 (16), 2248–2258. doi:10.1039/c4tb00125g

Potter-Baker, K. A., Stewart, W. G., Tomaszewski, W. H., Wong, C. T., Meador, W. D., Ziats, N. P., et al. (2015). Implications of chronic daily anti-oxidant administration on the inflammatory response to intracortical microelectrodes. *J. Neural Eng.* 12 (4), 046002. doi:10.1088/1741-2560/12/4/046002

Prasad, A., Xue, Q. S., Sankar, V., Nishida, T., Shaw, G., Streit, W. J., et al. (2012). Comprehensive characterization and failure modes of tungsten microwire arrays in chronic neural implants. *J. Neural Eng.* 9 (5), 056015. doi:10.1088/1741-2560/9/5/056015

Ravikumar, M., Sunil, S., Black, J., Barkauskas, D. S., Haung, A. Y., Miller, R. H., et al. (2014). The roles of blood-derived macrophages and resident microglia in the neuroinflammatory response to implanted Intracortical microelectrodes. *Biomaterials* 35 (28), 8049–8064. doi:10.1016/j.biomaterials.2014.05.084

Retterer, S. T., Smith, K., Bjornsson, C., Neeves, K., Spence, A., Turner, J., et al. (2004). Model Neural Prostheses With Integrated Microfluidics: A Potential Intervention Strategy for Controlling Reactive Cell and Tissue Responses. *IEEE Trans. Biomed. Eng.* 51 (11), 2063–2073. doi:10.1109/tbme.2004.834288

Rusek, M., Smith, J., El-Khatib, K., Aikins, K., Czuczwar, S. J., and Pluta, R. (2023). The Role of the JAK/STAT Signaling Pathway in the Pathogenesis of Alzheimer's Disease: new Potential Treatment Target. *Int. J. Mol. Sci.* 24 (1), 864. doi:10.3390/ijms24010864

Scherrmann, J. M. (2002). Drug delivery to brain via the blood–brain barrier. *Vasc. Pharmacol.* 38 (6), 349–354. doi:10.1016/s1537-1891(02)00202-1

Schwartz, A. B., Cui, X. T., Weber, D., and Moran, D. W. (2006). Brain-Controlled Interfaces: movement Restoration with Neural Prosthetics. *Neuron* 52 (1), 205–220. doi:10.1016/j.neuron.2006.09.019

Scott, S., and Ali, Z. (2021). Fabrication Methods for Microfluidic Devices: an Overview. *Micromachines* 12 (3), 319. doi:10.3390/mi12030319

Shanmuganathan, K., Capadona, J. R., Rowan, S. J., and Weder, C. (2010). Biomimetic mechanically adaptive nanocomposites. *Prog. Polym. Sci.* 35, 212–222. doi:10.1016/j.progpolymsci.2009.10.005

Shih, J. J., Krusienski, D. J., and Wolpaw, J. R. (2012). "Brain-computer interfaces in medicine," in *Mayo clinic proceedings* (Amsterdam, Netherlands: Elsevier Ltd), 268–279.

Shoffstall, A. J., Ecker, M., Danda, V., Joshi-Imre, A., Stiller, A., Yu, M., et al. (2018a). Characterization of the neuroinflammatory response to thiol-ene shape memory polymer coated intracortical microelectrodes. *Micromachines* 9 (10), 486. doi:10.3390/mi9100486

Shoffstall, A. J., Paiz, J. E., Miller, D. M., Rial, G. M., Willis, M. T., Menendez, D. M., et al. (2018b). Potential for thermal damage to the blood–brain barrier during craniotomy: implications for intracortical recording microelectrodes. *J. Neural Eng.* 15 (3), 034001–34001. doi:10.1088/1741-2552/aa9f32

Sridharan, A., Nguyen, J. K., Capadona, J. R., and Muthuswamy, J. (2015). Compliant intracortical implants reduce strains and strain rates in brain tissue *in vivo*. *J. Neural Eng.* 12 (3), 036002. doi:10.1088/1741-2560/12/3/036002

Szabo, E., and Hess-Dunning, A. (2021). Irreversible, self-aligned microfluidic packaging for chronic implant applications. *J. Micromechanics Microengineering* 31 (9), 095011. doi:10.1088/1361-6439/ac1994

Takabayashi, T., Vannier, E., Clark, B. D., Margolis, N. H., Dinarello, C. A., Burke, J. F., et al. (1996). A new biologic role for C3a and C3a desArg: regulation of TNF-alpha and IL-1 beta synthesis. *J. Immunol.* 156 (9), 3455–3460. doi:10.4049/jimmunol.156.9.3455

Takeuchi, S., Suzuki, T., Mabuchi, K., and Fujita, H. (2004). 3D flexible multichannel neural probe array. *J. Micromechanics Microengineering* 14 (1), 104–107. doi:10.1088/0960-1317/14/1/014

Takeuchi, S., Ziegler, D., Yoshida, Y., Mabuchi, K., and Suzuki, T. (2005). Parylene flexible neural probes integrated with microfluidic channels. *Lab a Chip* 5 (5), 519–523. doi:10.1039/b417497f

Takmakov, P., Ruda, K., Scott Phillips, K., Isayeva, I. S., Krauthamer, V., and Welle, C. G. (2015). Rapid evaluation of the durability of cortical neural implants using accelerated aging with reactive oxygen species. *J. Neural Eng.* 12 (2), 026003–26003. doi:10.1088/1741-2560/12/2/026003

Thakor, N. V. (2013). Translating the Brain-Machine Interface. *Sci. Transl. Med.* 5 (210), 210ps17. doi:10.1126/scitranslmed.3007303

Thompson, C. H., Saxena, A., Heelan, N., Salatino, J., and Purcell, E. K. (2021). Spatiotemporal patterns of gene expression around implanted silicon electrode arrays. *J. Neural Eng.* 18 (4), 045005. doi:10.1088/1741-2552/abf2e6

Tresco, P. A., and Winslow, B. D. (2011). The challenge of integrating devices into the central nervous system. *Crit. Rev. Biomed. Eng.* 39 (1), 29–44. doi:10.1615/critrevbiomedeng.v39.i1.30

Uchiyama, Y., Yanagisawa, K., Kunishima, S., Shiina, M., Ogawa, Y., Nakashima, M., et al. (2018). A novel CYCS mutation in the α-helix of the CYCS C-terminal domain causes non-syndromic thrombocytopenia. *Clin. Genet.* 94 (6), 548–553. doi:10.1111/cge.13423

Urwin, P. E., Lilley, C. J., and Atkinson, H. J. (2002). Ingestion of Double-Stranded RNA by Preparasitic Juvenile Cyst Nematodes Leads to RNA Interference. *Mol. Plant-Microbe Interactions®* 15 (8), 747–752. doi:10.1094/mpmi.2002.15.8.747

Usoro, J. O., Sturgill, B. S., Musselman, K. C., Capadona, J. R., and Pancrazio, J. J. (2021a). Intracortical Microelectrode Array Unit Yield under Chronic Conditions: A Comparative Evaluation. *Micromachines* 12 (8), 972. doi:10.3390/mi12080972

Usoro, J., Sturgill, B. S., Musselman, K. C., Capadona, J. R., and Pancrazio, J. J. (2021b). Intracortical Microelectrode Array Unit Yield under Chronic Conditions: A Comparative Evaluation. *Micromachines* 12 (8), 972. doi:10.3390/mi12080972

Wei, J., Liu, J., Liang, S., Sun, M., and Duan, J. (2020). Low-Dose Exposure of Silica Nanoparticles Induces Neurotoxicity via Neuroactive Ligand–Receptor Interaction Signaling Pathway in Zebrafish Embryos . *Int. J. Nanomedicine* 15, 4407–4415. doi:10.2147/ijn.s254480

Wester, B. A., Lee, R. H., and LaPlaca, M. C. (2009). Development and characterization of *in vivo* flexible electrodes compatible with large tissue displacements. *J. Neural Eng.* 6 (2), 024002–24002. doi:10.1088/1741-2560/6/2/024002

Xiromerisiou, G., Hadjigeorgiou, G. M., Papadimitriou, A., Katsarogiannis, E., Gourbali, V., and Singleton, A. B. (2008). Association between AKT1 gene and Parkinson's disease: A protective haplotype. *Neurosci. Lett.* 436 (2), 232–234. doi:10.1016/j.neulet.2008.03.026

Ziemba, A. M., Woodson, M. C. C., Funnell, J. L., Wich, D., Balouch, B., Rende, D., et al. (2022). Development of a Slow-Degrading Polymerized Curcumin Coating for Intracortical Microelectrodes. *ACS Appl. Bio Mater.* 6, 806–818. doi:10.1021/acsabm.2c00969